



# Influence of meteorology and anthropogenic pollution on chemical flux divergence of the NO–NO<sub>2</sub>–O<sub>3</sub> triad above and within a natural grassland canopy

Daniel Plake, Mathias Sörgel, Patrick Stella, Alexander Held, Ivonne Trebs

## ► To cite this version:

Daniel Plake, Mathias Sörgel, Patrick Stella, Alexander Held, Ivonne Trebs. Influence of meteorology and anthropogenic pollution on chemical flux divergence of the NO–NO<sub>2</sub>–O<sub>3</sub> triad above and within a natural grassland canopy. *Biogeosciences*, 2015, 12 (4), pp.945-959. 10.5194/bg-12-945-2015 . hal-01549619

**HAL Id: hal-01549619**

**<https://hal.science/hal-01549619>**

Submitted on 28 Jun 2017

**HAL** is a multi-disciplinary open access archive for the deposit and dissemination of scientific research documents, whether they are published or not. The documents may come from teaching and research institutions in France or abroad, or from public or private research centers.

L'archive ouverte pluridisciplinaire **HAL**, est destinée au dépôt et à la diffusion de documents scientifiques de niveau recherche, publiés ou non, émanant des établissements d'enseignement et de recherche français ou étrangers, des laboratoires publics ou privés.



# Influence of meteorology and anthropogenic pollution on chemical flux divergence of the NO–NO<sub>2</sub>–O<sub>3</sub> triad above and within a natural grassland canopy

D. Plake<sup>1,\*</sup>, M. Sörge<sup>1</sup>, P. Stella<sup>1,\*\*</sup>, A. Held<sup>2</sup>, and I. Trebs<sup>1,\*\*\*</sup>

<sup>1</sup>Max Planck Institute for Chemistry, Biogeochemistry Department, P.O. Box 3060, 55020 Mainz, Germany

<sup>2</sup>University of Bayreuth, Atmospheric Chemistry, Bayreuth, Germany

\* now at: Air Monitoring Department, UCL Umwelt Control Labor GmbH, 44536 Lünen, Germany

\*\* now at: AgroParisTech, UMR INRA/AgroParisTech SAD-APT, Paris, France

\*\*\* now at: Luxembourg Institute of Science and Technology, Environmental Research and Innovation (ERIN) Department, 4422 Belvaux, Luxembourg

Correspondence to: I. Trebs (ivonne.trebs@list.lu)

Received: 9 May 2014 – Published in Biogeosciences Discuss.: 14 July 2014

Revised: 19 December 2014 – Accepted: 23 December 2014 – Published: 17 February 2015

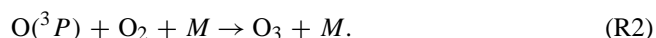
**Abstract.** The detailed understanding of surface–atmosphere exchange fluxes of reactive trace gases is a crucial precondition for reliable modelling of processes in atmospheric chemistry. Plant canopies significantly impact the atmospheric budget of trace gases. In the past, many studies focused on taller forest canopies or crops, where the bulk plant material is concentrated in the uppermost canopy layer. However, within grasslands, a land-cover class that globally covers vast terrestrial areas, the canopy structure is fundamentally different, as the main biomass is concentrated in the lowest part of the canopy. This has obvious implications for aerodynamic in-canopy transport, and consequently also impacts on global budgets of key species in atmospheric chemistry such as nitric oxide (NO), nitrogen dioxide (NO<sub>2</sub>) and ozone (O<sub>3</sub>).

This study presents for the first time a comprehensive data set of directly measured in-canopy transport times and aerodynamic resistances, chemical timescales, Damköhler numbers, trace gas and micrometeorological measurements for a natural grassland canopy (canopy height = 0.6 m). Special attention is paid to the impact of contrasting meteorological and air chemical conditions on in-canopy transport and chemical flux divergence. Our results show that the grassland canopy is decoupled throughout the day. In the lowermost canopy layer, the measured transport times are fastest during nighttime, which is due to convection during nighttime and a stable stratification during daytime in this layer. The inverse

was found in the layers above. During periods of low wind speed and high NO<sub>x</sub> (NO+NO<sub>2</sub>) levels, the effect of canopy decoupling on trace gas transport was found to be especially distinct. The aerodynamic resistance in the lowermost canopy layer (0.04–0.2 m) was around 1000 s m<sup>−1</sup>, which is as high as values determined previously for the lowest metre of an Amazonian rain forest canopy. The aerodynamic resistance representing the bulk canopy was found to be more than 3–4 times higher than in forests. Calculated Damköhler numbers (ratio of transport and chemical timescales) suggest a strong flux divergence for the NO–NO<sub>2</sub>–O<sub>3</sub> triad within the canopy during daytime. During that time, the timescale of NO<sub>2</sub> uptake by plants ranged from 90 to 160 s and was the fastest relevant timescale, i.e. faster than the reaction of NO and O<sub>3</sub>. Thus, our results reveal that grassland canopies of similar structure exhibit a strong potential to retain soil-emitted NO due to oxidation and subsequent uptake of NO<sub>2</sub> by plants. Furthermore, photo-chemical O<sub>3</sub> production was observed above the canopy, which was attributed to a deviation from the NO–NO<sub>2</sub>–O<sub>3</sub> photostationary state by a surplus of NO<sub>2</sub> due to oxidation of NO, by e.g. peroxy radicals. The O<sub>3</sub> production was one order of magnitude higher during high NO<sub>x</sub> than during low NO<sub>x</sub> periods and resulted in an underestimation of the O<sub>3</sub> deposition flux measured with the EC method.

## 1 Introduction

Nitric oxide (NO) and nitrogen dioxide (NO<sub>2</sub>) play a crucial role in air chemistry as they act as key catalysts for ozone (O<sub>3</sub>) production and are therefore involved in the generation of hydroxyl radicals (OH) (Crutzen, 1973). The most significant tropospheric source of O<sub>3</sub> is initiated by photochemical dissociation of NO<sub>2</sub> and subsequent reaction of the oxygen (O) atom with molecular oxygen:



In the case that O<sub>3</sub> is present, it may oxidize NO and re-form NO<sub>2</sub>:



In the absence of additional reactions, R1–R3 represent a null cycle. Besides R1–R3, NO is oxidized by peroxy radicals (HO<sub>2</sub>+RO<sub>2</sub>), which constitutes an important net O<sub>3</sub> production pathway in the troposphere (Warneck, 2000).

Dry deposition to terrestrial surfaces, especially to plant canopies, is an important sink for tropospheric O<sub>3</sub> and NO<sub>2</sub>. The uncertainties of dry deposition estimates are substantially higher for NO<sub>2</sub>, because its net ecosystem exchange can be bi-directional depending on the ambient NO<sub>2</sub> levels (Lerdau et al., 2000). O<sub>3</sub> instead is exclusively deposited to surfaces. In contrast, NO is known to be mainly net emitted from nearly all soil types. Biogenic NO soil emissions contribute about 20 % to the global NO<sub>x</sub> (NO+NO<sub>2</sub>) emissions (IPCC, 2013), highlighting the need of detailed investigations on NO<sub>x</sub> soil–atmosphere exchange.

A major challenge for studies investigating surface–atmosphere exchange fluxes of these reactive trace gases is the presence of plant canopies. These significantly modify the aerodynamic properties of the surface and, thus, alter trace gas exchange fluxes. Most previous studies focused on taller canopies such as forests. However, grassland canopies represent a highly important land cover class covering globally 41 % and Europe-wide 19 % of the terrestrial land surface (Suttie et al., 2005; Kasanko et al., 2011). In contrast to forests, grasslands feature the main bulk plant area density near the soil (e.g. Ripley and Redman, 1976; Jäggi et al., 2006), accompanied with mean distances between plant elements of only some millimetres (Aylor et al., 1993). Organized coherent structures govern turbulence dynamics within and above plant canopies (Finnigan, 2000). The mean in-canopy transport is slower than above the canopy (e.g. Nemitz et al., 2009). This modification of in-canopy transport has important implications for global atmospheric chemistry. Plant canopies and the soil below are biologically actively emitting and taking up reactive trace gases, and conditions

within canopies may provide sufficient time for fast chemical reactions (Nemitz et al., 2009). Subsequently, they modify surface exchange fluxes (e.g. Rinne et al., 2012). For instance, ammonia can be released by a part of the canopy and taken up by another (Nemitz et al., 2000; Denmead et al., 2007). In addition, recapturing of NO<sub>2</sub> originating from biogenic soil NO emissions after reaction with O<sub>3</sub> within plant canopies (Rummel et al., 2002) is accounted for in global models by a so-called canopy reduction factor for NO<sub>x</sub> (Yienger and Levy, 1995). However, these estimates are based on only one single experiment in an Amazonian rain forest (Bakwin et al., 1990), and a subsequent model analysis (Jacob and Wofsy, 1990). Canopy reduction for grasslands and other ecosystems has not been experimentally studied up to now. The contrasting canopy structure of grassland and forest ecosystems highlights the need for a detailed analysis and an evaluation of the suggested NO<sub>x</sub> canopy reduction factor of e.g. 64 % by Yienger and Levy (1995) for temperate grassland.

Net ecosystem exchange fluxes are typically measured at a certain height above the canopy. They rely on the constant flux layer assumption (e.g. Swinbank, 1968), which however, may be violated for reactive trace gases within or just above the vegetation. To assess the potential chemical divergence of exchange fluxes, the Damköhler number (*DA*) has commonly been applied (e.g. Rinne et al., 2012). *DA* is calculated as the ratio of the transport time ( $\tau_{\text{tr}}$ ) and the characteristic chemical timescale ( $\tau_{\text{ch}}$ ):

$$DA = \frac{\tau_{\text{tr}}}{\tau_{\text{ch}}}. \quad (1)$$

Hence, *DA* above unity indicates that chemical reactions occur significantly faster than the transport (flux divergence), whereas *DA* smaller than 0.1 indicates the reverse case. The range in between is commonly addressed as a critical range, where an impact of chemistry cannot be excluded (Stella et al., 2013).

In this paper, we present directly measured transport times, chemical timescales and corresponding Damköhler numbers for three layers above and within a natural grassland canopy under contrasting meteorological and air chemical conditions. For the first time, such a comprehensive analysis involving trace gas and micrometeorological measurements is made for a grassland canopy. Furthermore, the consequences of in-canopy processes for NO<sub>x</sub> canopy reduction and simultaneously measured O<sub>3</sub> deposition fluxes will be discussed.

## 2 Material and methods

### 2.1 Site description

We performed an intensive field experiment from July to September 2011 at the estate of the Mainz Finthen Airport in Rhineland-Palatinate, Germany (further details given in

Plake and Trebs, 2013; Plake et al., 2014; Moravek et al., 2014, 2015). The vegetation at the site was nutrient-poor grassland with a mean canopy height ( $h_c$ ) of 0.6 m and a leaf area index (LAI) of  $4.8 \text{ m}^2 \text{ m}^{-2}$ . A list of species and an LAI profile are given in Plake et al. (2014), with the latter indicating a high biomass density below 0.2 m corresponding to 85 % of the total LAI. Topographically located on a plateau 150 m above the Rhine valley, the site is located about 9 km south-west of the city centre of Mainz. The site is surrounded by villages and motorways in a distance of 2 to 6 km and 4 to 15 km, respectively. The surrounding area is mainly characterized by agricultural use for vineyards, orchards and crops. The fetch is largest in southwestern direction without significant anthropogenic pollution sources.

## 2.2 Experimental setup

A vertical Thoron (Tn) profile system was operated at  $z_1 = 0.04$ ,  $z_2 = 0.2$  and  $z_3 = 0.8$  m for the direct determination of transport times (for details see Plake and Trebs, 2013). Vertical profiles of NO, NO<sub>2</sub>, O<sub>3</sub> and CO<sub>2</sub> were measured at  $z_1$ ,  $z_2$ ,  $z_3$  and additionally at  $z_4 = 4.0$  m by a system described in detail by Plake et al. (2014). Briefly, NO was measured by detection of the chemiluminescence produced during the reaction of NO and O<sub>3</sub> (TEI 42iTL Thermo Scientific, Waltham, USA). NO<sub>2</sub> was photolytically converted to NO by exposure of the sample air to a blue light converter (BLC, Droplet Measurement Technologies, Boulder, USA). O<sub>3</sub> mixing ratios were measured with a UV-absorption analyser (TEI-49i, Thermo Scientific, Waltham, USA). The efficiency of the photolytic conversion of NO<sub>2</sub> to NO was determined by a back-titration procedure involving the reaction of O<sub>3</sub> with NO using a gas phase titration system (SYCOS K-GPT, Ansycos GmbH, Karlsruhe, Germany). Details on the sampling schedule and time resolution of the trace gas profiles system are described in Plake et al. (2014).

This study is based on simultaneous operation of both vertical profile systems at identical heights and, thus, focuses on the period from 19 August to 26 September 2011 when both systems were operational. Vertical profiles of temperature (HMT337, Vaisala, Helsinki, Finland), wind speed and direction (WS425, Vaisala, Helsinki, Finland) were installed at 0.2, 0.8, 1.5, 2.5, 4.0 m. Soil temperature (107L, Campbell Scientific Inc., Logan, USA) was measured at  $-0.02$  m. Global radiation ( $G$ ) and the NO<sub>2</sub> photolysis frequency ( $j_{\text{NO}_2}$ ) were measured at a height of 2.5 m with a net radiometer (CNR1, Kipp & Zonen, Delft, Netherlands), and a filter radiometer (Meteorology Consult GmbH, Königstein, Germany), respectively. The data of temperature, wind and radiation were recorded by a data logger (CR3000, Campbell Scientific) every 10 s. A 3-D sonic anemometer (CSAT-3, Campbell Scientific) placed at  $z_{\text{ref}} = 3.0$  m measured 3-D wind and temperature at 20 Hz and the data were recorded by a CR3000 data logger. The friction velocity ( $u_*$ ) and stability functions ( $z/L$ ) were computed using the TK3 software

(see Mauder and Foken, 2011). Eddy covariance fluxes of O<sub>3</sub> were simultaneously measured and are described in detail by Plake et al. (2014).

## 2.3 Theory

The data analysis was carried out for three individual layers ( $L_{1-3}$ ), which are named in ascending order starting at the soil surface. Hence,  $L_1$  is the lowermost canopy layer between the corresponding measurement heights  $z_{1-2}$  ( $\Delta z(L_1) = 0.16$  m),  $L_2$  the upper canopy layer between  $z_{2-3}$  ( $\Delta z(L_2) = 0.6$  m), and  $L_3$  the layer above the canopy between  $z_3$  and  $z_{\text{ref}}$  ( $\Delta z(L_3) = 2.2$  m). As shown in Plake et al. (2014) the vertical trace gas gradients between  $z_{\text{ref}}$  and  $z_4$  were negligible, allowing the use of mixing ratios measured at  $z_4$  for  $L_3$ .

### 2.3.1 Chemical timescales

The overall chemical timescale  $\tau_{\text{ch}}$  (in s) of the NO–NO<sub>2</sub>–O<sub>3</sub> triad (Lenschow, 1982) was calculated for each layer ( $L_i$ ,  $i = 1, 2, 3$ ) as

$$\tau_{\text{ch}}(L_i) = 2 / \left\{ j_{\text{NO}_2}(L_i)^2 + k_3(L_i)^2 \times (N_{\text{O}_3}(L_i) - N_{\text{NO}}(L_i))^2 + 2j_{\text{NO}_2}(L_i) \times k_3(L_i) \times (N_{\text{O}_3}(L_i) + N_{\text{NO}}(L_i) + 2N_{\text{NO}_2}(L_i)) \right\}^{0.5}, \quad (2)$$

where  $N_{\text{O}_3}$ ,  $N_{\text{NO}}$  and  $N_{\text{NO}_2}$  are the number densities (in molecules  $\text{cm}^{-3}$ ) of O<sub>3</sub>, NO and NO<sub>2</sub> for  $L_{1-3}$ , and  $k_3$  the reaction rate constant of Reaction (R3) (in  $\text{cm}^3 \text{ molecule}^{-1} \text{ s}^{-1}$ ) according to Atkinson et al. (2004). Geometric means of the number densities at  $z_{1-4}$  were used in Eq. (2) to account for non-linear profiles – e.g.  $N_{\text{NO}}(L_1) = \sqrt{N_{\text{NO}}(z_1) \times N_{\text{NO}}(z_2)}$ .

Equation (2) gives the chemical timescale of Reactions (R1) and (R3) derived from the O<sub>3</sub> chemical-budget equation, i.e. considering only the reactions between O<sub>3</sub>, NO and NO<sub>2</sub> and not taking into account reactions of other compounds (e.g. peroxy radicals and VOCs). It is defined as the time at which the mixing ratio of one of the compounds significantly changes from its initial value when reacting with the other ones. It can also be seen as the time required for reaching a new photostationary state following a change in O<sub>3</sub>, NO or NO<sub>2</sub> mixing ratios, or the reaction rate constants  $j_{\text{NO}_2}$  and  $k_3$  (see Ganzeveld et al., 2012). The underlying assumptions are:

- only source and sink terms of the “triad” are considered, which means other reactions (e.g. RO<sub>2</sub> + NO) are not included;
- covariance terms and other budget terms i.e. horizontal and vertical advection, flux divergence and change in O<sub>3</sub> mixing ratio  $d[\text{O}_3]/dt$  are neglected.

### 2.3.2 NO<sub>2</sub> photolysis within the canopy

The data gaps in the measured time series of  $j_{\text{NO}_2}$  (in s<sup>-1</sup>) above the canopy were filled using the parameterization of  $j_{\text{NO}_2}$  as a function of  $G$  (in W m<sup>-2</sup>) by Trebs et al. (2009). This approach was also used to parameterize in-canopy  $j_{\text{NO}_2}$  from a vertical in-canopy profile of  $G$ . The latter was calculated as a function of the LAI profile using the method of Monsi and Saeki (1953):

$$G(\text{LAI}) = G_0 \times \exp^{(-k_{\text{ex}} \times \text{LAI})}, \quad (3)$$

where  $G_0$  (in W m<sup>-2</sup>) is the above-canopy  $G$  and  $k_{\text{ex}}$  is the dimensionless extinction coefficient of the canopy. In this study, the extinction coefficient of barley ( $k_{\text{ex}} = 0.69$  by Monteith and Unsworth, 1990) was used. First  $G(\text{LAI})$  was deduced and then converted into  $j_{\text{NO}_2}$ . Finally, geometric means of  $j_{\text{NO}_2}$  were calculated for  $j_{\text{NO}_2}(L_{1-3})$ .

### 2.3.3 Transport times

For  $L_3$ , height-integrated transport times  $\tau_{\text{tr}}(L_3)$  (in s) were derived by multiplying the aerodynamic resistance  $R_a(L_3)$  (e.g. Hicks et al., 1987; Erisman et al., 1994) with the layer thickness  $\Delta z(L_3)$  (see Stella et al., 2013):

$$\tau_{\text{tr}}(L_3) = R_a(L_3) \times \Delta z(L_3) \quad (4)$$

$$R_a(L_3) = \frac{1}{\kappa \times u_*} \left[ \ln \left( \frac{z_{\text{ref}} - d}{z_3 - d} \right) - \Psi_H \left( \frac{z_{\text{ref}} - d}{L} \right) + \Psi_H \left( \frac{z_3 - d}{L} \right) \right], \quad (5)$$

where  $\kappa$  is the von Kàrmàn constant ( $= 0.4$ ),  $d$  the displacement height ( $d = 0.75 \times h_c$ ),  $\Psi_H$  the stability correction function for heat (Foken, 2008) and  $L$  the Obukhov length.

In the canopy,  $\tau_{\text{tr}}(L_i, i = 1, 2)$  were derived from the vertical Tn profiles (Lehmann et al., 1999; Plake and Trebs, 2013):

$$\tau_{\text{tr}}(L_i) = \ln \left[ \frac{C_{\text{Tn}_{z_l}}(L_i)}{C_{\text{Tn}_{z_u}}(L_i)} \right] / \lambda \quad (6)$$

where  $C_{\text{Tn}_{z_l}}$  and  $C_{\text{Tn}_{z_u}}$  are the measured Tn concentrations (in Bq m<sup>-3</sup>) at the lower ( $z_l$ ) and upper ( $z_u$ ) heights of  $L_i$ , and  $\lambda$  the radioactive decay rate  $\lambda = \ln 2 / T_{0.5} = 0.0125 \text{ s}^{-1}$  (Hänsel and Neumann, 1995).

## 3 Results

### 3.1 Meteorological conditions and mixing ratios

During the field experiment, low and high NO<sub>x</sub> periods occurred that were directly coupled to the wind direction and could be attributed to two contrasting synoptic conditions characterized by different wind speeds (see Moravek et al.,

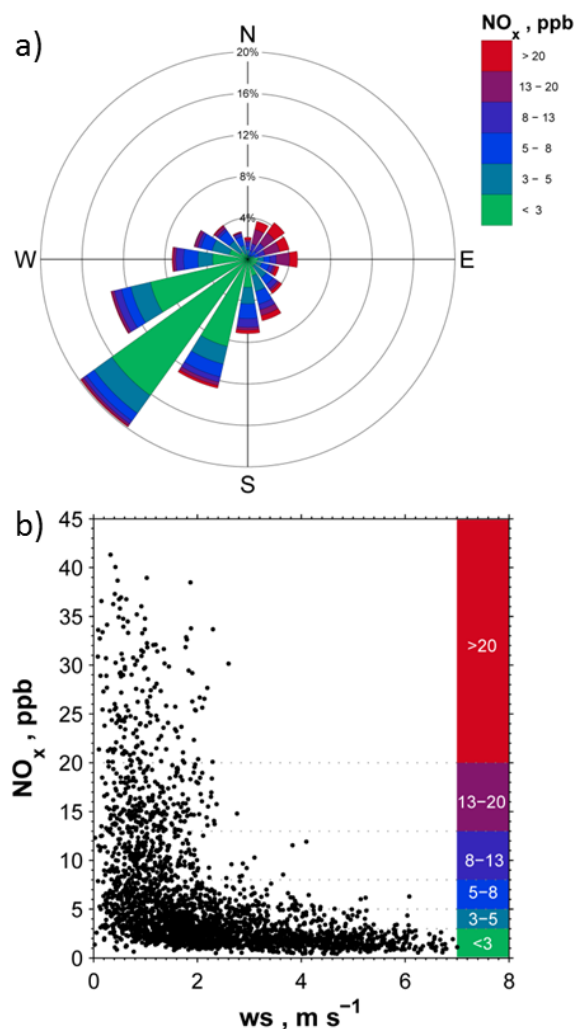


**Figure 1.** (a) Frequency distribution of wind direction related to NO<sub>x</sub> mixing ratios; (b) NO<sub>x</sub> mixing ratios as function of wind speed at the Mainz Finthen grassland site.

2015). Figure 1a displays the dominance of southwesterly winds at the site during 45 % of the field experiment and their relation to relatively low NO<sub>x</sub> levels ( $< 3$  ppb). Contrastingly, winds from the northeastern sector were characterized by high NO<sub>x</sub> levels often above 13 ppb (Fig. 1a). High NO<sub>x</sub> episodes (up to 40 ppb) were accompanied with low wind speed ( $< 3 \text{ m s}^{-1}$ ) and low NO<sub>x</sub> ( $< 5$  ppb) with wind speeds above  $3 \text{ m s}^{-1}$  as shown in Fig. 1b. O<sub>3</sub> levels exhibited the opposite dependency on wind speed, while the measured CO<sub>2</sub> levels generally showed a similar pattern for high and low NO<sub>x</sub> levels.

For further data analysis, defined criteria made it possible to account for these specific relationships. In order to clearly separate entire days (24 h) of contrasting conditions from each other, the criteria were defined as low NO<sub>x</sub> or high NO<sub>x</sub> periods when (i) the mean daytime wind speed was  $> 3 \text{ m s}^{-1}$  and the wind direction mainly ranged between 180 and 270°,

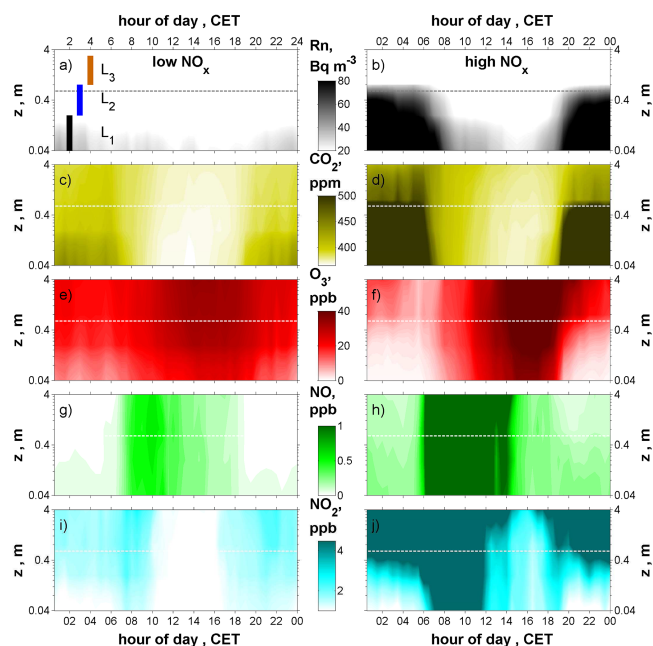


**Figure 2.** Time height cross-sections indicating the median vertical distribution of (a, b) Rn, (c, d) CO<sub>2</sub>, (e, f) O<sub>3</sub>, (g, h) NO and (i, j) NO<sub>2</sub> during low NO<sub>x</sub> (left panels) and high NO<sub>x</sub> (right panels) conditions at the Mainz Finthen grassland site. The canopy height (dotted line) and L<sub>1–3</sub> are also shown. The plots were made using the *contourf* function of MATLAB.

or (ii) the mean daytime wind speed was  $< 3 \text{ m s}^{-1}$  and the wind direction was mainly outside  $180\text{--}270^\circ$ , respectively. The wind direction definition was fulfilled during 96 % of the low NO<sub>x</sub> periods and during 84 % of the high NO<sub>x</sub> periods. Following these criteria, we identified 11 and 9 days as low and high NO<sub>x</sub> periods, respectively, which were analysed separately.

### 3.2 Vertical profiles of trace gases

Since the wind field drives vertical exchange of scalars such as trace gases between vegetation and the atmosphere (Finnigan, 2000), it affects their vertical distribution. Passive tracers such as Rn and CO<sub>2</sub> are used especially at nighttime as indicators for vertical exchange processes within plant canopies (e.g. Trumbore et al., 1990; Nemitz et al., 2009). Generally, nighttime wind speeds during the low and high NO<sub>x</sub> periods were accordingly higher and lower, respectively. This was reflected by the in-canopy concentrations of both Rn and CO<sub>2</sub> (Fig. 2a–d). During nighttime when both gases are exclusively emitted by soil, a rather weak enrichment within the canopy (Fig. 2a, c) reflected higher wind speeds and, thus, enhanced exchange during the low NO<sub>x</sub> periods. In comparison, during the high NO<sub>x</sub> periods a strong in-canopy CO<sub>2</sub> and Rn accumulation was observed (Fig. 2b, d). During daytime, photosynthesis prohibits the use of CO<sub>2</sub> as passive tracer, whereas Rn profiles are still useful as no

biological processes such as stomatal uptake affect its concentration (Lehmann et al., 1999). The vertical exchange is generally enhanced during daytime causing dilution of the in-canopy Rn concentrations, which was especially pronounced during the low NO<sub>x</sub> periods (Fig. 2a) and was less evident during the high NO<sub>x</sub> periods (Fig. 2b) with generally lower wind speeds.

The vertical distribution of O<sub>3</sub> (Fig. 2e, f) reflected a typical pattern with lower mixing ratios closer to the ground and higher mixing ratios above. The diurnal O<sub>3</sub> maximum occurred during the afternoon around 16:00 CET (= UTC +1). Nevertheless, in the low NO<sub>x</sub> periods the diurnal O<sub>3</sub> maximum was much less pronounced compared to the high NO<sub>x</sub> periods with 35 and 50 ppb, respectively. Furthermore, characteristic vertical O<sub>3</sub> distributions were observed during the low and high NO<sub>x</sub> periods. Nighttime O<sub>3</sub> gradients were less pronounced during the low NO<sub>x</sub> than during the high NO<sub>x</sub> periods. Median in-canopy values of O<sub>3</sub> were 10–20 ppb and were 20–25 ppb above the canopy during the low NO<sub>x</sub> periods (Fig. 2e). During the high NO<sub>x</sub> periods 1–6 ppb of O<sub>3</sub> were measured in the canopy and 10–25 ppb above the canopy (Fig. 2f).

During both the low and the high NO<sub>x</sub> periods, significantly enhanced NO mixing ratios prevailed during the morning hours from 06:00 to 14:00 CET (Fig. 2g, h) with median diurnal maxima of 0.6 and 7.2 ppb, respectively, both occurring at 10:00 CET (not visible in Fig. 2h due to scaling). The NO mixing ratios decreased afterwards to approach nighttime minima. These were characterized by small vertical NO gradients during both periods. During low NO<sub>x</sub> nights, NO appeared to be mainly present in the in-canopy air layer, with median mixing ratios at  $z_1$  and  $z_2$  of  $\leq 0.1$  ppb. The median values at  $z_1$  and  $z_2$  during the high NO<sub>x</sub> periods were  $\leq 0.3$  ppb, respectively.

NO<sub>2</sub> mixing ratios were generally found to increase with height (Fig. 2i, j), featuring significantly stronger vertical differences during the high NO<sub>x</sub> periods. Similar to NO, also NO<sub>2</sub> mixing ratios were enhanced throughout the profile during the morning hours of both, low and high NO<sub>x</sub> periods, with corresponding values of 1–2.5 ppb and 6–14 ppb, respectively. At nighttime, comparable NO<sub>2</sub> mixing ratios of around 1 ppb prevailed during both periods at  $z_1$ . NO<sub>2</sub> showed stronger gradients above the canopy during the high NO<sub>x</sub> periods. The diurnal NO<sub>2</sub> minima during low and high NO<sub>x</sub> periods were observed between 12–16 CET and 14–16 CET, respectively.

### 3.3 Vertical profiles of chemical timescales

The obtained values for  $\tau_{\text{ch}}$  were generally higher during nighttime than during daytime (Fig. 3a, d, g) and increased from L<sub>3</sub> to L<sub>1</sub>. The validity of our applied criteria for separation between low and high NO<sub>x</sub> periods is shown by the median values (brown and green lines) that nearly adjoin the interquartile range of the overall data set. Significantly higher



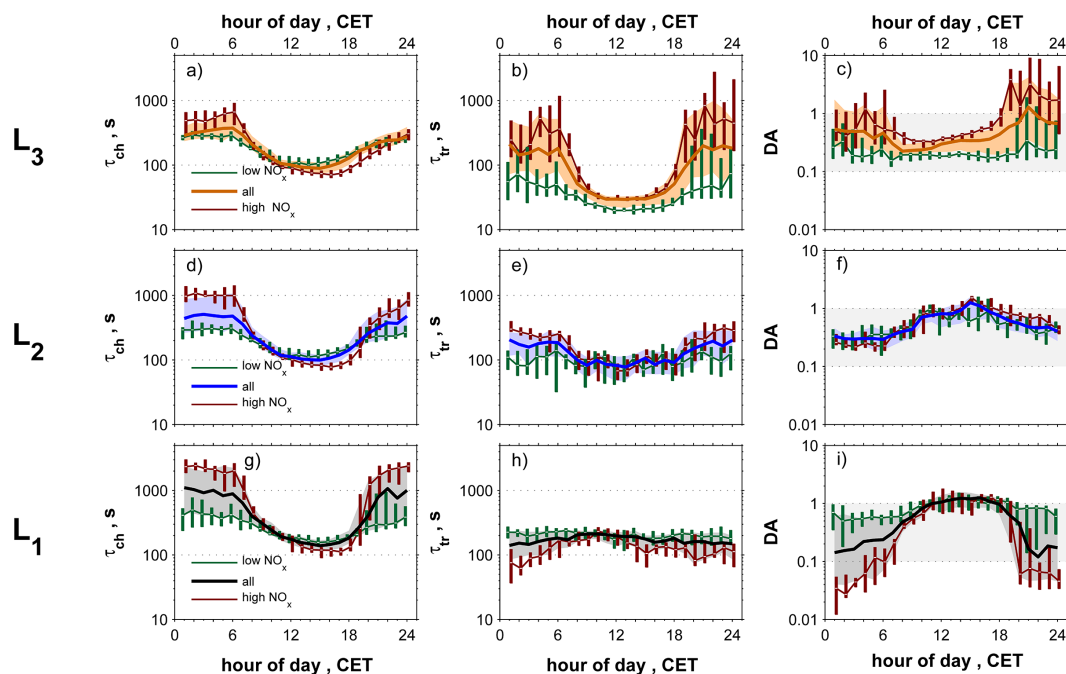


**Figure 3.** Diurnal courses of (a, d, g)  $\tau_{ch}(L_{1-3})$ , (b, e, h)  $\tau_{tr}(L_{1-3})$  and (c, f, i)  $DA(L_{1-3})$  considering all data from 19 August to 26 September 2011 (medians and shaded interquartile ranges) and the low  $NO_x$  and high  $NO_x$  periods (green and brown medians and interquartile boxes) at the Mainz Finthen grassland site.

$\tau_{ch}$  values prevailed during nighttime of the high  $NO_x$  periods, ranging from 300 to 2500 s in  $L_{1-3}$ . In contrast, low  $NO_x$  periods were characterized by  $\tau_{ch}$  of 250–800 s in  $L_{1-3}$ . However, during daytime  $\tau_{ch}$  was within 100–200 s in  $L_{1-3}$  for both periods. During the low  $NO_x$  periods  $\tau_{ch}$  values were slightly higher compared to the high  $NO_x$  periods.

### 3.4 Vertical profiles of transport times

The median  $\tau_{tr}(L_3)$  of all data (Fig. 3b) was one order of magnitude smaller during noon than at midnight with 30 and 200 s, respectively. As for  $\tau_{ch}$  (Sect. 3.3), also in the case of  $\tau_{tr}$  the medians of the low and high  $NO_x$  periods adjoined the interquartile range of the overall data set. For example,  $\tau_{tr}(L_3)$  in the low  $NO_x$  periods never exceeded  $\tau_{tr}(L_3)$  in the high  $NO_x$  periods (see Fig. 3b). The difference of  $\tau_{tr}(L_3)$  between noon and midnight was largest in the high  $NO_x$  and smallest during the low  $NO_x$  periods with 470 and 40 s, respectively. Compared to  $L_{1-2}$  (Fig. 3e, h), the extreme values of the entire  $\tau_{tr}$  data set were found above the canopy in  $L_3$ . The overall  $\tau_{tr}$  minimum occurred during daytime of the low  $NO_x$  periods, and the maximum during nighttime of the high  $NO_x$  periods in  $L_3$ .

The diurnal course of  $\tau_{tr}(L_2)$  from the entire data set in Fig. 3e exhibited a similar pattern as  $\tau_{tr}(L_3)$ , with higher  $\tau_{tr}(L_2)$  during nighttime than during daytime. Representative nighttime and daytime values were 200 and 100 s, respec-

tively, and a similar nighttime separation between the low and high  $NO_x$  periods as in Fig. 3b is observed.

In contrast, both diurnal  $\tau_{tr}(L_1)$  medians representing all data and the high  $NO_x$  periods (Fig. 3h) were slightly higher during daytime between 08:00 and 13:00 CET than at nighttime with around 200 and 75–175 s, respectively. During the low  $NO_x$  periods, the median  $\tau_{tr}(L_1)$  was relatively constant throughout the day with about 200 s. The pattern of  $\tau_{tr}(L_1)$  was generally opposite to  $L_{2-3}$ , with faster  $\tau_{tr}(L_1)$  in the high  $NO_x$  periods than in the low  $NO_x$  periods.

### 3.5 Vertical profiles of Damköhler numbers

The values for  $DA(L_3)$  presented in Fig. 3c were generally smaller during daytime than during nighttime. They exhibited a diurnal minimum of 0.2 and a maximum of 1.3 at 08:00 and 21:00 CET, respectively. During the low  $NO_x$  periods, the difference of the  $DA(L_3)$  median ( $0.2 < DA(L_3) < 0.3$ ) to a  $DA$  of unity was highest, whereas in the high  $NO_x$  periods  $DA(L_3)$  remained at higher median values ( $0.3 < DA(L_3) < 3.9$ ).

In contrast, the diurnal course of  $DA(L_2)$  in Fig. 3f exhibited its maximum of 1.25 at 15:00 CET and featured nighttime minima of about 0.3. The difference in  $DA(L_2)$  between the low and high  $NO_x$  periods was not as pronounced as for  $DA(L_3)$ . This was most obvious from 15:00 to 24:00 CET with lower  $DA(L_2)$  in the low  $NO_x$  periods. Hence, both

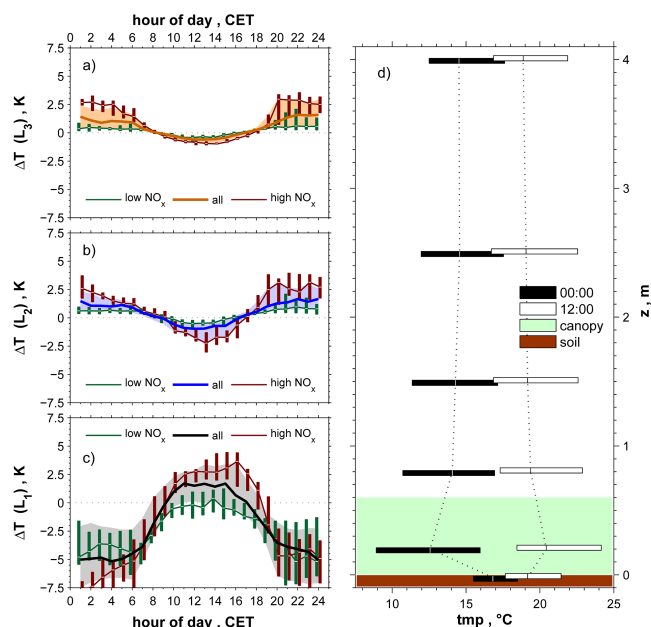


**Figure 4.** (a–c) Diurnal courses of measured  $\Delta T(L_1-3)$  considering all data from 19 August to 26 September 2011 (medians and shaded interquartile ranges) and the low and high NO<sub>x</sub> periods (green and brown medians and interquartile ranges); note:  $\Delta T(L_1, L_3)$  do not fully cover  $L_1$  and  $L_3$  (Sect. 2.3) due to availability of measurements (Sect. 2.2); (a)  $\Delta T(L_3)$ : 2.5–0.8 m; (b)  $\Delta T(L_2)$ : 0.8–0.2 m; (c)  $\Delta T(L_1)$ : 0.2 to –0.02 m (soil temperature). (d) Median vertical temperature profiles and interquartile boxes representing the thermal stratification at 00:00 and 12:00 CET considering all data from 19 August to 26 September 2011 at the Mainz Finthen grassland site.

$DA(L_{2,3})$  values throughout the day were within or above the critical range for  $DA$  under all conditions.

Interestingly, the diurnal course of  $DA(L_1)$  (Fig. 3i) nearly mirrored that of  $DA(L_3)$ , with highest and lowest  $DA$  during daytime and nighttime, respectively. The diurnal median of  $DA(L_1)$  partly exhibited values below 0.1 (transport dominates) during nighttime of the high NO<sub>x</sub> periods, values above unity (chemistry dominates) from 12:00 to 17:00 CET under all conditions, and between 0.1 and unity during nighttime in the overall data set and in the low NO<sub>x</sub> periods.

## 4 Discussion

### 4.1 Transport times and resistances

#### 4.1.1 Thermal stratification

The diurnal courses of the temperature differences  $\Delta T(L_1-3)$  in Fig. 4a–c describe the stability in each layer. They clearly indicate contrasting stability conditions in  $L_1$  and  $L_{2-3}$ . During daytime, negative values of  $\Delta T(L_{2-3})$  reflected unstable conditions, while positive

$\Delta T(L_1)$  reflected stable conditions. In contrast, at nighttime these conditions were reversed. Similar diurnal cycles of stratifications are observed for other canopies (see Jacobs et al., 1994; Kruijt et al., 2000; Nemitz et al., 2000), and are known to decouple the lower canopy from the air layers above (see Fig. 4d). Canopy coupling regimes are typically classified according to the detection of coherent structures in high frequency time series of scalars such as temperature (e.g. Foken et al., 2012; Dupont and Patton, 2012). In our data set  $\Delta T(L_1)$  was used to explain why  $\tau_{tr}(L_1)$  was generally smaller, i.e. transport was faster during nighttime than during daytime (Fig. 3h). The soil released stored heat as thermal plumes during nighttime that drove an in-canopy nighttime convection, which reached up to the height of the temperature inversion as found by Dupont and Patton (2012) or Jacobs et al. (1994). The  $\tau_{tr}(L_1)$  maximum of 200 s from 08:00 to 13:00 CET could accordingly be attributed to positive  $\Delta T(L_1)$  values at that time indicating a stable stratification. The thermal stratification was stronger during the high NO<sub>x</sub> periods and weaker during the low NO<sub>x</sub> periods in all layers (Fig. 4a–c). This was caused by higher wind speeds during the low NO<sub>x</sub> periods causing increased turbulence and mixing that yielded smaller vertical temperature differences.

#### 4.1.2 Aerodynamic resistances and transport times

Aerodynamic resistances above ( $R_a$ ) and within the canopy ( $R_{ac}$ ) are considered as important input variables for modelling studies on surface–atmosphere exchange fluxes. They can be derived from the transport times through a layer, normalized by the layer thickness ( $R_{a(c)} = \tau_{tr}/\Delta z$ ). In cases when the thicknesses of two layers under consideration differ, the effectiveness of transport can be represented by the corresponding aerodynamic resistances. On the other hand, transport times are required to evaluate the influence of chemical reactions on fluxes (e.g.  $DA$ ).

Typically,  $R_{ac}$  values are parameterized as a function of  $u_*$  and LAI (e.g. van Pul and Jacobs, 1994; Personne et al., 2009). These parameterizations are based on experiments above, e.g. crops such as maize (van Pul and Jacobs, 1994), and consider a vertically homogeneous leaf distribution (Personne et al., 2009). However, this approximation may differ substantially within grassland canopies, as their structure is characterized by high biomass density in the lowest layer (see Sect. 2.1).

The importance of our results is underlined by the direct assessment of measured  $R_{ac}$  values. From Eq. (6) we can assess  $R_{ac}$  for different canopy layers ( $L_1$ ,  $L_2$  and for the whole canopy ( $\tau_{tr}(z_1, z_3)$ ;  $\Delta z = z_3 - z_1$ )) of the grassland (see Fig. 5). In the lowermost canopy layer,  $R_{ac}(L_1)$  was generally highest with medians of 900 to 1000 s m<sup>−1</sup> during nighttime and 1000 to 1300 s m<sup>−1</sup> during daytime (Fig. 5). In comparison, Gut et al. (2002) found the aerodynamic resistance in the lowest metre of an Amazonian rain forest



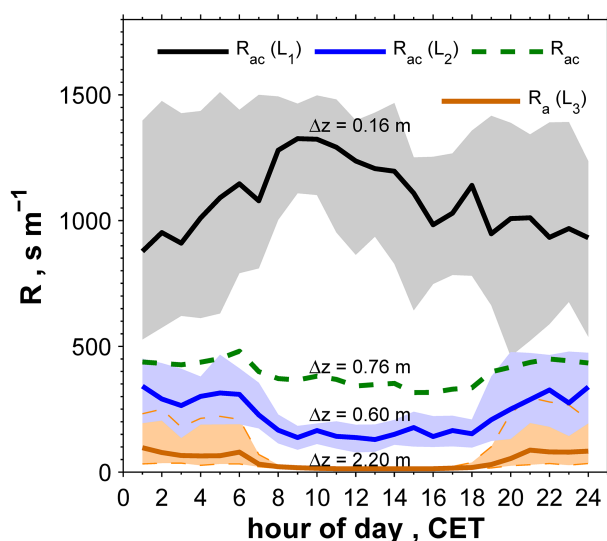


**Figure 5.** Diurnal courses of in-canopy aerodynamic resistances for each individual canopy layer ( $R_{ac}(L_1)$ ,  $R_{ac}(L_2)$ ) and for the entire grassland canopy ( $R_{ac} = \frac{\tau_{tr}(L_1) + \tau_{tr}(L_2)}{z_3 - z_1}$ ) at the Mainz Finthen site (median and shaded interquartile ranges). For comparison, the aerodynamic resistance above the canopy is also displayed ( $R_a(L_3)$ ). The layer thickness ( $\Delta z$ ) is indicated. The plot includes all data from 19 August until 26 September 2011.

canopy in a similar range with  $600 \text{ s m}^{-1}$  during nighttime and  $1700 \text{ s m}^{-1}$  during daytime, showing the same diurnal pattern.

As found for the transport times, the diurnal course of  $R_{ac}$  in the upper layers mirrored that of the lowermost layer (Fig. 5). In the upper canopy, the median of  $R_{ac}(L_2)$  typically ranged around  $300 \text{ s m}^{-1}$  during nighttime and around  $150 \text{ s m}^{-1}$  during daytime. In comparison, above the canopy the median of  $R_a(L_3)$  (Eq. 5) was substantially lower with around  $80$  and  $15 \text{ s m}^{-1}$  during nighttime and daytime, respectively. Consequently, the aerodynamic resistances in and above the canopy ( $R_{ac}(L_{1,2})$  and  $R_a(L_3)$ ) differed by almost two orders of magnitude during daytime, and by one order of magnitude during nighttime. Accordingly, the efficiency of aerodynamic transport decreased with decreasing height, even if the transport times were occasionally shorter in  $L_1$  compared to  $L_3$ .  $R_{ac}$  for the entire canopy (Fig. 5) reflects the sum of the measured transport times divided by the entire layer thickness ( $\Delta z = z_3 - z_1$ ) and can be considered as equivalent to a weighted average of  $R_{ac}(L_1)$  and  $R_{ac}(L_2)$ .  $R_{ac}$  ranged in-between  $R_{ac}(L_1)$  and  $R_{ac}(L_2)$  with  $440 \text{ s m}^{-1}$  during nighttime and  $360 \text{ s m}^{-1}$  during daytime. The opposite diurnal courses of both  $R_{ac}(L_1)$  and  $R_{ac}(L_2)$  have an impact on  $R_{ac}$ , which in turn showed a smaller diurnal variation. As  $L_2$  contained around 80 % of the layer thickness between  $z_1$  and  $z_3$  (see Fig. 5),  $R_{ac}$  was closer to  $R_{ac}(L_2)$ .

The median transport time through the 0.6 m high natural grassland canopy (also referred to as “canopy flushing time”)

was presented in the related study of Plake and Trebs (2013) for the same experiment. It was measured using the vertical thoron profile between  $z_1$  and  $z_3$  (Eq. 6). The canopy flushing time is consistent with the sum of  $\tau_{tr}(L_1)$  and  $\tau_{tr}(L_2)$  in this paper (see Fig. 7) and represents the in-canopy layer down to  $0.07 \times h_c$  ( $z_1/h_c$ ). It was determined to be  $\leq 6$  min exhibiting only small daytime/nighttime variation. Simon et al. (2005) reported canopy flushing times of around 60 min during any time of the day based on radon measurements within a 40 m high rain forest canopy for the layer between  $h_c$  and  $0.13 \times h_c$  (canopy top to trunk space). As in the grassland canopy in Mainz Finthen, nighttime in-canopy convection accounted for the small daytime/nighttime variation in their study. Normalization of their canopy flushing time by the layer thickness yielded  $R_{ac}$  of the order of  $100 \text{ s m}^{-1}$ , which is around 3–4 times lower than the corresponding  $R_{ac}$  of the grassland site. Other studies (Holzinger et al., 2005; Rummel, 2005) based on surface renewal models reported somewhat lower flushing times. Rummel (2005) found flushing times in a 32 m high rain forest canopy of  $\leq 200 \text{ s}$  during daytime, which correspond to  $R_{ac}$  values  $\leq 10 \text{ s m}^{-1}$ . In the same way Holzinger et al. (2005) determined flushing times of 90 s during daytime and around 300 s during nighttime within a 6 m high scrubby pine forest. Corresponding  $R_{ac}$  values were of the order of 20 and  $60 \text{ s m}^{-1}$ , respectively.

Thus, it is important to note that even if the canopy height of natural grassland canopies is small compared to forests (around 1–10 %); the corresponding canopy flushing times are within the same order of magnitude as those reported for forest canopies. The typically high biomass density in the lower canopy of grasslands (e.g. Jäggi et al., 2006; Nemitz et al., 2009) is the most obvious explanation. It provides a large aerodynamic resistance ( $> 900 \text{ s m}^{-1}$ ) in a small layer adjacent to the ground (here:  $R_{ac}(L_1)$ ). This resistance is large enough to increase the overall aerodynamic resistance of the whole canopy ( $R_{ac}$ ) by 50 and 140 % during night and daytime, respectively. Consequently,  $R_{ac}$  of the grassland canopy was found to be at least 3–4 times higher than  $R_{ac}$  values representing corresponding in-canopy layers of forests taken from the literature.

Plake and Trebs (2013) compared their directly measured transport times with the parameterizations of van Pul and Jacobs (1994) and Personne et al. (2009). They found that none of the parameterizations was able to reproduce the entire diurnal course of the in-canopy transport. Agreement with the measured transport times was either found during daytime (Personne et al., 2009) or nighttime (van Pul and Jacobs, 1994), underlining the need for more direct measurements of in-canopy transport.

## 4.2 Chemical timescales

The non-linear profiles of  $\text{NO}$ ,  $\text{NO}_2$  and  $\text{O}_3$  might have introduced uncertainties in  $\tau_{ch}(L_{1-3})$ . The potential uncertainties due to averaging were investigated by determining the

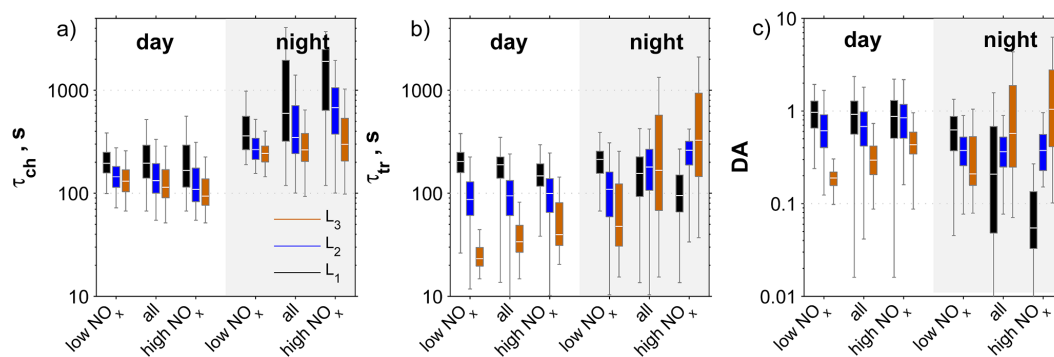


**Figure 6.** Comparison of box plot statistics for  $\tau_{\text{ch}}(L_{1-3})$ ,  $\tau_{\text{tr}}(L_{1-3})$  and  $DA(L_{1-3})$  during daytime and nighttime including all data from 19 August until 26 September 2011 separated for the low and high  $\text{NO}_x$  periods at the Mainz Finthen grassland site.

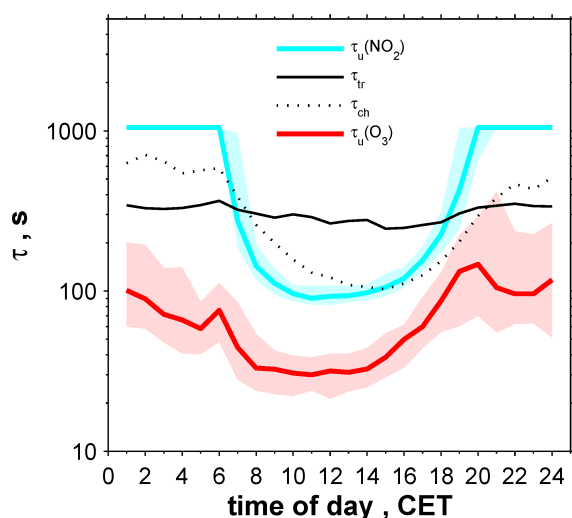


**Figure 7.** Comparison of median diurnal  $\tau_{\text{u}}(\text{NO}_2)$ ,  $\tau_{\text{u}}(\text{O}_3)$ ,  $\tau_{\text{tr}}$  and  $\tau_{\text{ch}}$  with interquartile ranges for the whole canopy layer ( $L_{1+2}$ ) considering all data from 19 August to 26 September 2011 at the Mainz Finthen grassland site.

individual  $\tau_{\text{ch}}(z_{1-4})$  and their subsequent comparison with  $\tau_{\text{ch}}(L_{1-3})$ . In  $L_1$ ,  $L_2$  and  $L_3$  they were found to be  $\leq 13$ ,  $\leq 4$  and  $\leq 2$  %, respectively, during daytime under any condition. During nighttime, the uncertainties in  $L_2$  and  $L_3$  were found to be 6 and 2 % during the low  $\text{NO}_x$  periods and 57 and 13 % during the high  $\text{NO}_x$  periods, respectively. In  $L_1$  the uncertainty during nighttime was 30 % for all conditions. Furthermore, the in-canopy parameterization of  $j_{\text{NO}_2}$  might have introduced additional uncertainties since (i) in reality the attenuation of in-canopy radiation might be more complex than described in Eq. (3), and (ii) the parameterization of  $j_{\text{NO}_2}$  from  $G$  is prone to uncertainties of  $> 40$  % for  $G < 100 \text{ W m}^{-2}$ , 10–40 % for  $G = 100\text{--}500 \text{ W m}^{-2}$  and  $\leq 10$  % for  $G > 500 \text{ W m}^{-2}$  (Trebs et al., 2009). Moreover, omitting the influence of peroxy radical ( $\text{HO}_2 + \text{RO}_2$ ) levels for the calculation of the chemical timescales introduces

uncertainties. However, measurements of vertical profiles of  $\text{HO}_2 + \text{RO}_2$  inside and above the grassland canopy are challenging and were not made during our experiment. Additionally, no straightforward analytical framework exists to calculate their influence on chemical timescales due to the variety of compounds and reaction rates involved in the complex  $\text{HO}_2 / \text{RO}_2$  chemistry, which would require numeral modelling (see Heal et al., 2001).

The diurnal maxima and minima of  $\tau_{\text{ch}}(L_{1-3})$  (Fig. 3a, d, g) were found to coincide with the  $\text{O}_3$  minima and maxima (Fig. 2e, f), respectively. The impact of the terms in Eq. (2) on  $\tau_{\text{ch}}(L_3)$  was examined by a correlation coefficient analysis. It was found to be highest for  $\text{O}_3$  followed by  $\text{NO}_2$  and  $\text{NO}$  with  $r = -0.57$ ,  $r = 0.46$  and  $r = -0.07$ , respectively. Consequently, the chemical timescale is dominated by the influence of  $\text{O}_3$  as long as  $\text{O}_3$  is present in excess compared to the other compounds. As the average air-chemical conditions in Mainz Finthen were characterized by a surplus of  $\text{O}_3$  compared to  $\text{NO}_2$  or  $\text{NO}$  (see Sect. 3.2), the magnitude of  $\tau_{\text{ch}}(L_3)$  was most affected by the mixing ratios of  $\text{O}_3$ . In contrast,  $\text{NO}$  was generally less abundant, which explained the low overall impact on  $\tau_{\text{ch}}(L_3)$ . Only during high  $\text{NO}_x$  periods, when  $\text{NO}$  levels were above 5 ppb (see Sect. 3.1), was an increased impact of  $\text{NO}$  on  $\tau_{\text{ch}}(L_3)$  found.

Figure 6a summarizes the chemical timescales. The temporal variation in  $\tau_{\text{ch}}$ , expressed by higher nighttime and lower daytime values, can be considered as a rather typical pattern based on the diurnal courses of  $\text{NO}$ ,  $\text{NO}_2$  and  $\text{O}_3$  (Fig. 2e–j) and their strong photochemical link. The vertical variation in  $\tau_{\text{ch}}(L_{1-3})$  was on the one hand caused by the attenuation of  $j_{\text{NO}_2}$  in the canopy, and on the other hand by generally increasing mixing ratios of  $\text{NO}$ ,  $\text{NO}_2$  and  $\text{O}_3$  with height (Fig. 2e–j). It should be noted that the latter finding is exclusively valid for this experimental site. Plake et al. (2014) measured insignificant soil biogenic  $\text{NO}$  emissions, underlined by weak in-canopy  $\text{NO}$  gradients (Fig. 2g, h). As already discussed in the previous paragraph, generally low  $\text{NO}$ ,  $\text{NO}_2$  and  $\text{O}_3$  mixing ratios tend to cause high  $\tau_{\text{ch}}$  values and vice versa. Consequently, at a site with higher  $\text{NO}$

emissions, such as an intensively managed agricultural field, the vertical  $\tau_{\text{ch}}$  profile would most likely feature smaller vertical differences.

The extremely high  $\tau_{\text{ch}}(L_1)$  during nighttime of the high  $\text{NO}_x$  periods (Fig. 6a) were a direct consequence of canopy decoupling (see Sect. 4.1.1). Transport of  $\text{O}_3$  and  $\text{NO}_2$  into the lower canopy was suppressed by the temperature inversion (see Fig. 2f, j). The residual  $\text{O}_3$  and  $\text{NO}_2$  molecules were convectively circulated within the lower canopy and subsequently deposited efficiently to surfaces until both almost disappeared in the early morning (Fig. 2f, j). Consequently, both the negligible  $\text{NO}$  emissions and the suppressed supply of  $\text{O}_3$  and  $\text{NO}_2$  from above yielded very low mixing ratios of all three trace gases, that in turn led to the very high  $\tau_{\text{ch}}(L_1)$  values.

Our results are in line with those of Stella et al. (2013) who reported median diurnal  $\tau_{\text{ch}}$  of 80–300 and 150–600 s above and within the canopy, respectively, for an intensively managed meadow. Their in-canopy  $\tau_{\text{ch}}$  maximum was somewhat lower than in Mainz Finthen, which might be attributed to  $\text{NO}$  soil emissions or to averaging of different layers.

As mentioned above, the chemistry of  $\text{HO}_2/\text{RO}_2$  is not considered in our study. The reaction rate constant of  $\text{NO} + \text{HO}_2/\text{RO}_2$  is about 500 times higher than that of the reaction  $\text{NO} + \text{O}_3$ . Assuming relatively high average daytime  $\text{HO}_2 + \text{RO}_2$  mixing ratios of 60 ppt inside the canopy (see Wolfe et al., 2014) the oxidation of  $\text{NO}$  to  $\text{NO}_2$  would be as fast as with 30 ppb of  $\text{O}_3$ . This implies that these chemical timescales may be comparable to those of the reaction  $\text{NO} + \text{O}_3$ , which dominates  $\tau_{\text{ch}}$  derived from Eq. (2). However, it should be noted that peroxides have a high affinity to be lost at surfaces, which may reduce their presence in dense grassland canopies. Additionally, reactions between volatile organic compounds (VOCs) and  $\text{O}_3$  (e.g. Atkinson and Arey, 2003) might have influenced chemical timescales. Simultaneously measured biogenic VOC mixing ratios featured very small values at our site (e.g. isoprene < 0.7 ppb, monoterpene < 0.3 ppb, J. Kesselmeier, personal communication, 2013). Due to the absence of measurements the influence of anthropogenic VOCs is not taken into account.

### 4.3 Influence of meteorology and air pollution on vertical Damköhler number profiles

The summarized daytime  $DA(L_{1-3})$  in Fig. 6c exhibited decreasing  $DA$  values with increasing layer height. Thus, the likelihood of chemical flux divergence decreased from  $L_1$  to  $L_3$ . Throughout  $L_1$  to  $L_3$ , the  $\tau_{\text{ch}}$  values (Fig. 6a) showed a lower variation compared to the corresponding  $\tau_{\text{tr}}$  values (Fig. 6b). Hence, the daytime  $DA$  profile was mainly caused by the vertical  $\tau_{\text{tr}}$  profile.

Interestingly, the nighttime  $DA$  for all data and the high  $\text{NO}_x$  periods showed opposite vertical profiles, indicating an increasing likelihood of chemical flux divergence with increasing layer height ( $L_1$  to  $L_3$ ). This was especially pro-

nounced during nighttime of the high  $\text{NO}_x$  periods, where the only instance without indication for a flux divergence within the entire data set for  $L_1$  was found. The reasons for this were (i) the very high  $\tau_{\text{ch}}(L_1)$  (Fig. 6a and Sect. 4.2), and (ii) the reversed vertical transport time profiles during nighttime (fastest in  $L_1$ ) of the high  $\text{NO}_x$  periods (Fig. 6b). This finding agrees very well with Rummel (2005) who found that the transport timescale in the lowermost layer of an Amazonian rainforest is faster than the chemical timescale of the  $\text{NO}-\text{NO}_2-\text{O}_3$  triad during nighttime.

Above the canopy, the order of magnitude (Fig. 6c) and the median diurnal course (Fig. 3c) of  $DA$  compared well with the values of Stella et al. (2013). The in-canopy  $DA$  of Stella et al. (2013) was smaller than the  $DA$  above the canopy throughout the entire day, which is in contrast to our study. Considering the average canopy flushing time given in Plake and Trebs (2013) (see Sect. 4.1.2) and the  $\tau_{\text{ch}}(L_2)$  (see Fig. 6a), the average in-canopy  $DA$  in Mainz Finthen was in the order of 2 and 1 for daytime and nighttime, respectively. Thus, in our study in-canopy  $DA$  values are on average significantly higher than above the canopy throughout the day. Finally, it should be noted that in-canopy  $DA$  values may not be fully representative as besides transport and chemistry, additional sources and sinks for trace gases exist within plant canopies. These are specific for each trace gas and will be further discussed below.

## 4.4 Implications for measured fluxes

### 4.4.1 Potential $\text{NO}_x$ canopy reduction

Within the canopy,  $DA(L_{1-2})$  (Fig. 3f, i; Fig. 6c) suggest that chemical reactions exhibited a larger influence on the  $\text{NO}-\text{NO}_2-\text{O}_3$  triad during daytime than during night. However, reactive trace gases in canopies are deposited to soil and vegetation elements. Trace gases can be efficiently taken up by plants due to adsorption/absorption on cuticles and diffusion through stomata (e.g. Breuninger et al., 2012). On the other hand, particularly  $\text{NO}$  is simultaneously produced by microbial processes and is subsequently released from soil. Although the latter process could be neglected in this study due to insignificant  $\text{NO}$  soil emissions (Sect. 4.2), the uptake of  $\text{NO}_2$  by plants, however, was investigated in order to draw conclusions on potential  $\text{NO}_x$  canopy reduction within natural grasslands canopies. Hence, the characteristic timescale of plant uptake ( $\tau_{\text{u}}$ ) of  $\text{NO}_2$  integrated over the whole canopy ( $L_{1+2}$ ) was estimated based on a resistance model (Baldocchi, 1988), following an approach of Rummel (2005) as

$$\tau_{\text{u}}(x) = \left( \frac{1}{R_{L_x}} \times \frac{\Delta LAI}{\Delta z} \right)^{-1}, \quad (7)$$

where  $x$  denotes the trace gas of interest (here  $x = \text{NO}_2$ ) and  $R_{L_x}$  is the leaf resistance of  $x$ :

$$R_{L_x} = \left( \frac{1}{R_{\text{bl}_x} + R_{\text{s}_x} + R_{\text{mes}_x}} + \frac{2}{R_{\text{bl}_x} + R_{\text{cut}_x}} \right)^{-1}, \quad (8)$$

with  $R_{bl_x}$  being the leaf boundary layer resistance of  $x$  calculated according to Personne et al. (2009),  $R_{s_x}$  the stomatal resistance of  $x$  taken from Plake et al. (2014),  $R_{mes_x}$  the mesophyll resistance set to  $200 \text{ s m}^{-1}$  for  $\text{NO}_2$  and  $R_{cut_x}$  the cuticular resistance set to  $9999 \text{ s m}^{-1}$  due to the unimportance of cuticular deposition for  $\text{NO}_2$  (both values were taken from Stella et al., 2013).

During daytime, the median of  $\tau_u(\text{NO}_2)$  calculated from all data was typically found to be the shortest amongst all timescales relevant for  $\text{NO}_2$ , typically ranging between 90 and 160 s between 09:00 and 17:00 CET (Fig. 7). This timescale was closely followed by  $\tau_{ch}(L_{1+2})$  exhibiting values between 100 and 200 s in the same time period, but the minimum was slightly skewed towards the afternoon. In contrast, the canopy flushing time,  $\tau_{tr}(L_{1+2})$ , ranged from 250 to 290 s (Fig. 7) during this time. For a comparable natural grassland canopy with significant NO soil emissions, this would imply an efficient in-canopy conversion of NO to  $\text{NO}_2$  during daytime, followed by an effective  $\text{NO}_2$  plant uptake as the transport was found to be 2–3 times slower. Furthermore, the biomass density within the lowest 0.2 m of the canopy (i) strongly inhibits the transport, especially in  $L_1$  during daytime (Figs. 5; 6b), and (ii) attenuates the photolysis of  $\text{NO}_2$  at the soil–canopy interface, the location where NO is usually emitted. This indicates that a strong potential for  $\text{NO}_x$  canopy reduction exists in such grassland ecosystems during daytime, when the precondition of significant NO soil emissions is fulfilled. The presence of peroxy radicals may even amplify this process.

However, during nighttime,  $\tau_u(\text{NO}_2)$  was found to be very large (Fig. 7) due to plant stomata closure. Hence, the role of turbulence–chemistry interactions ( $DA(L_{1-2})$ ) was dominating over biological uptake processes. In  $L_1$  the transport of soil emitted NO would be slowest under relatively windy nighttime situations (low  $\text{NO}_x$  periods in Fig. 3h) due to undeveloped in-canopy convection. Thus, a considerably high mixing ratio of  $\text{O}_3$  within the canopy (Fig. 2e) would lead to an efficient formation of  $\text{NO}_2$  indicated by  $DA(L_{1-2})$  close to unity. The uptake of  $\text{NO}_2$  by plants would be insignificant (see above), and only soil deposition would lead to a small  $\text{NO}_2$  depletion. Most likely, such nighttime conditions would lead to simultaneous  $\text{NO}_2$  and NO canopy emission fluxes. During nights with low wind speeds (high  $\text{NO}_x$  periods), the temperature inversion constitutes a “canopy lid”. Within the canopy ( $L_{1+2}$ ) the reaction of residual  $\text{O}_3$  (see Sect. 4.2) and soil-emitted NO would compete with the  $\text{O}_3$  deposition to surfaces. Subsequently, a mixture of NO and  $\text{NO}_2$  would be trapped inside the canopy. Besides some minor in-canopy  $\text{NO}_2$  losses (see above), a distinct NO and  $\text{NO}_2$  release may occur in the morning hours, which has been observed for forests (see Foken et al., 2012; Dorsey et al., 2004; Jacob and Wofsy, 1990).

#### 4.4.2 Influence on $\text{O}_3$ deposition flux

Similar to  $\text{NO}_2$ , the application of in-canopy  $DA$  values for  $\text{O}_3$  remains difficult, since plant uptake and deposition to plant surfaces and the soil are additional  $\text{O}_3$  loss pathways. The characteristic timescale of  $\text{O}_3$  plant uptake and soil deposition  $\tau_u(\text{O}_3)$ , shown in Fig. 7, was estimated using Eqs. (7) and (8), with  $x = \text{O}_3$ ,  $R_{mes_x}$  set to  $0 \text{ s m}^{-1}$  (Erisman et al., 1994) and  $R_{cut_x} = R_{ns_x} - R_{soil_x}$  (e.g. Lamaud et al., 2009). The  $R_{ns_x}$  was taken from Plake et al. (2014) and  $R_{soil_x} = 240 \text{ s m}^{-1}$  according to Lamaud et al. (2009). The  $\tau_u(\text{O}_3)$  ranged from 30 to 150 s, which clearly illustrates the dominance of in-canopy  $\text{O}_3$  plant uptake and soil deposition. The  $\tau_u(\text{O}_3)$  was significantly faster than both  $\tau_{tr}(L_{1-2})$  and  $\tau_{ch}(L_{1-2})$  during the entire day (values are given in Sect. 4.4.1).

Consequently, only  $DA$  values above the canopy, i.e.  $DA(L_3)$ , provide an indication for potential  $\text{O}_3$  flux divergence. Since the  $DA(L_3)$  always exceeded 0.1 (Figs. 3c, 6c), a chemical flux divergence could not be excluded at the Mainz Finthen site. Furthermore,  $DA > 1$  (Fig. 3c) during the early evening hours clearly indicated the dominance of chemical reactions over transport. During the low  $\text{NO}_x$  periods, the probability for flux divergence was lowest. The influence of chemistry on  $\text{O}_3$  deposition fluxes determined by Plake et al. (2014) at the Mainz Finthen grassland site will be discussed below. The median  $\text{O}_3$  fluxes for the entire measurement period ranged from about  $-1.5$  to  $-6 \text{ nmol m}^{-2} \text{ s}^{-1}$  during night and daytime, respectively.

Due to negligible NO soil emissions, a chemical flux divergence in  $L_3$  resulting from counter-directed fluxes of NO and  $\text{O}_3$  was very unlikely. Nevertheless, we use a simplified method proposed by Duyzer et al. (1995) based on R1 and R3 and the law of mass conservation to approximate the flux divergence by the correction factor  $\alpha_{\text{O}_3}$  as

$$\alpha_{\text{O}_3} = \frac{\phi_x}{\kappa \times u_*} \times [k_1 \times (N_{\text{NO}} \times F_{\text{O}_3}^* + N_{\text{O}_3} \times F_{\text{NO}}^*) - j_{\text{NO}_2} \times F_{\text{NO}_2}^*], \quad (9)$$

where  $\phi_x = \phi_{\text{O}_3} = \phi_{\text{H}}$  was the stability correction function for heat (Högström, 1988),  $F_{\text{O}_3}^*$  the measured  $\text{O}_3$  flux at  $z_{\text{ref}}$  determined by the eddy covariance method (see Plake et al., 2014) and  $F_{\text{NO}}^*$  and  $F_{\text{NO}_2}^*$  the corresponding NO and  $\text{NO}_2$  fluxes determined by the dynamic chamber technique (see Plake et al., 2014). The estimated  $\text{O}_3$  deposition flux at  $z_3$  ( $F_{z_3}$ ) was then calculated as

$$F_{z_3} = F_{z_{\text{ref}}} + \int_{z_3}^{z_{\text{ref}}} \left( \frac{\partial F}{\partial z} \right) dz = F_{\text{O}_3}^* + \alpha_{\text{O}_3} \times z_3 \times \left( 1 + \ln \frac{z_{\text{ref}}}{z_3} \right), \quad (10)$$

where the term  $\int_{z_3}^{z_{\text{ref}}} \left( \frac{\partial F}{\partial z} \right) dz$  is the integrated flux divergence within  $L_3$ . The resulting median  $\text{O}_3$  flux divergence was quantified to be less than 1 %, confirming our a priori assumption.

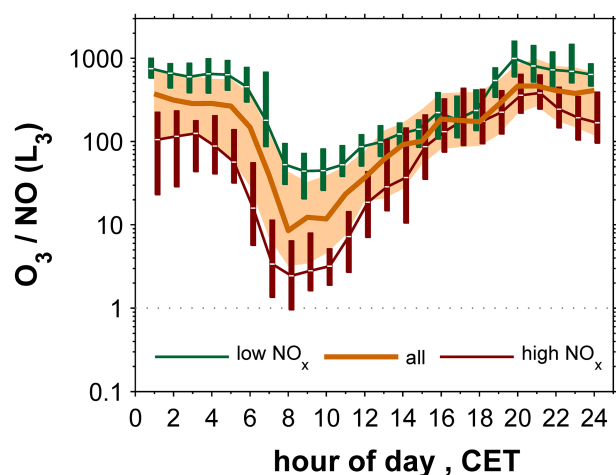


**Figure 8.** Diurnal course of the  $O_3$  to  $NO$  ratio in  $L_3$  considering all data from 19 August to 26 September 2011 (median and shaded interquartile range) and separated for the low  $NO_x$  and high  $NO_x$  periods (medians and interquartile boxes) at the Mainz Finthen grassland site.

Nevertheless, we examined the influence of the enhanced  $NO$  mixing ratios in the morning hours (Sect. 3.2, Fig. 2g, h), accompanied by very low  $O_3/NO$  ratios (Fig. 8) on the measured  $O_3$  fluxes. A chemically induced  $O_3$  flux  $F_c(O_3)$  due to production  $P(O_3)$  or loss  $L(O_3)$  of  $O_3$  by Reactions (R1) and (R3) integrated over the air column of  $L_3$  was quantified according to Rummel et al. (2007) as

$$F_c(O_3) = P(O_3) - L(O_3) = \int_{z_3}^{z_{ref}} \frac{\mu_{NO_2}(z) \times \rho_d(z)}{\tau_{NO_2}(z)} dz - \int_{z_3}^{z_{ref}} \frac{\mu_{O_3}(z) \times \rho_d(z)}{\tau_{O_3}(z)} dz, \quad (11)$$

where  $\rho_d$  (in  $\text{mol m}^{-3}$ ) is the molar density of dry air.  $\tau_{NO_2}$  and  $\tau_{O_3}$  (in s) are the chemical depletion times of  $NO_2$  and  $O_3$ , respectively:

$$\tau_{NO_2} = \frac{1}{j_{NO_2}} \quad (12)$$

$$\tau_{O_3} = \frac{1}{k_1 \times N_{NO}}. \quad (13)$$

Figure 9a displays the diurnal courses of  $P(O_3)$  and  $L(O_3)$  exhibiting median values of 0 to  $1.9 \text{ nmol m}^{-2} \text{ s}^{-1}$  and 0 to  $-1.4 \text{ nmol m}^{-2} \text{ s}^{-1}$ , respectively. The maximal median values were related to the enhanced  $NO_x$  levels in the morning. The resulting median net  $F_c(O_3)$  in Fig. 9b ranged between 0.6 and  $-0.05 \text{ nmol m}^{-2} \text{ s}^{-1}$ , representing a net  $O_3$  production in  $L_3$  during daytime and a net loss during nighttime. Repeatedly, the medians of low and high  $NO_x$  periods

adjoined the interquartile range of the overall data set, showing a variability of one order of magnitude of net  $F_c(O_3)$  during daytime. Considering the median values of all data, the chemical contribution to the measured EC flux of  $O_3$  would be around +10 % during daytime and -3 % during nighttime. Consequently, the actual daytime  $O_3$  deposition to the canopy is higher than measured by the EC method. This finding is interesting, as to our knowledge previous studies only reported chemical  $O_3$  losses above the canopy due to outbalancing of the reactions of  $O_3$  with  $NO$  (e.g. Dorsey et al., 2004) or VOCs (e.g. Kurpius and Goldstein, 2003) emitted by soil or plants, respectively. The net  $O_3$  production in our study was attributed to a deviation from the  $NO$ – $NO_2$ – $O_3$  photostationary state by a surplus of  $NO_2$  due to  $NO$  oxidation by e.g., peroxy radicals or other oxidants (see Trebs et al., 2012). Unfortunately, we were not able to assess the impact of the reactions involved in the net  $O_3$  production on the calculated chemical timescales as measurements of peroxy radicals were not available. The  $NO_2$  surplus might have originated from simultaneous emissions of non-methane hydrocarbons, carbon monoxide (CO) and  $NO$  from motorways surrounding the site in a distance of some kilometres. It is well known that under daytime conditions peroxy radicals are formed that can oxidize  $NO$  without consumption of  $O_3$  resulting in net  $O_3$  production (Seinfeld and Pandis, 2006). Although this  $O_3$  production might also prevail at other experimental sites, this effect is most likely balanced or even exceeded by the destruction of  $O_3$  due to biogenic soil  $NO$  emissions which were negligible at our site (a nutrient-poor grassland site).

## 5 Conclusions

For the first time, we simultaneously measured transport times (aerodynamic resistances), vertical profiles of  $NO$ – $NO_2$ – $O_3$  mixing ratios and micrometeorological quantities within and above a natural grassland canopy. The obtained data were analysed to gain insights about the potential  $NO_x$  canopy reduction in the grassland canopy, and to analyse the contribution of chemistry on fluxes of purely depositing compounds, such as  $O_3$ . We observed two extreme regimes: (a) high wind speed and low  $NO_x$  mixing ratios (low  $NO_x$  periods) and (b) low wind speed and high  $NO_x$  mixing ratios (high  $NO_x$  periods). Our study highlights that as a result of in-canopy convection, nighttime transport in the lowermost canopy layer is fastest, while conditions above the canopy are highly stable due to low wind speed during the high  $NO_x$  periods.

Interestingly, our results on transport-chemistry interactions within the grassland canopy are partly comparable to those found in the Amazonian rainforest, although the vertical canopy structure differs substantially. Natural grasslands exhibit very high biomass densities in the lowest part of the canopy. Thus, the median aerodynamic resistance in the low-



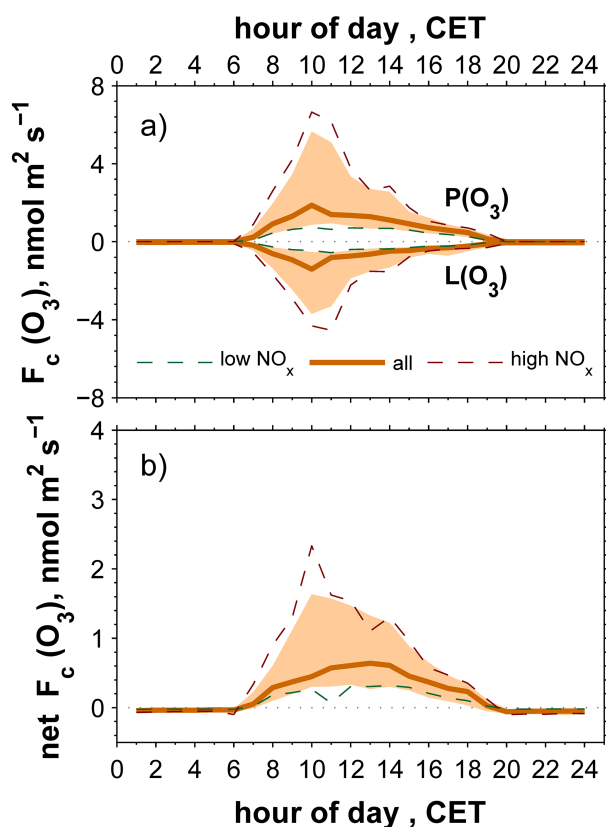


**Figure 9.** Diurnal courses showing (a)  $P(O_3)$  and  $L(O_3)$  and (b)  $F_c(O_3)$  (Eq. 11) for  $L_3$  considering all days from 19 August to 26 September 2011 (medians and shaded interquartile ranges) and separated for the low and high  $NO_x$  periods (medians) at the Mainz Finthen grassland site.

ermost canopy layer (0.04–0.2 m) was found to be of the same magnitude ( $> 900 \text{ s m}^{-1}$ ) and to feature the same diurnal pattern (higher during daytime, lower at night) as the aerodynamic resistance determined for the lowest metre of an Amazonian rain forest. The median in-canopy aerodynamic resistance representing the whole grassland canopy was at least 3–4 times higher than in-canopy aerodynamic resistances of forest canopies available from the literature. Our results reveal that even if the canopy height of natural grassland canopies is small compared to forests (around 1–10 %), the corresponding canopy flushing times are of the same order of magnitude as those reported for forest canopies. The median canopy flushing times exhibited only small daytime/nighttime variability, which is in accordance with a detailed study on flushing times within an Amazonian rain forest (Simon et al., 2005). The small daytime/nighttime variability is caused by the compensating transport efficiencies in the lower and upper canopy layers during daytime and nighttime for both canopy types.

The median canopy flushing time of the grassland was found to be  $\leq 6$  min and the chemical timescale of the  $NO$ –

$NO_2$ – $O_3$  triad during daytime ranged between 1–3 min. This has obvious implications, e.g. for soil-emitted reactive compounds such as  $NO$ , potentially implying fast chemical conversion of  $NO$  to  $NO_2$  within the grassland canopy. During daytime the plant uptake of  $NO_2$  was shown to be 2–3 times faster than the canopy flushing time. Inevitably, this leads to a strong potential  $NO_x$  canopy reduction in the presence of biogenic  $NO$  soil emissions. This effect may be amplified if substantial levels of peroxy radicals prevail inside the canopy. Due to the extensive global terrestrial coverage with grassland canopies, this finding is highly relevant for the application of global chemistry and transport models. Our results indicate that the daytime  $NO_x$  canopy reduction for grasslands may be higher than 64 %. Nevertheless, an improved daily average for the  $NO_x$  canopy reduction factor in analogy to Yienger and Levy (1995) cannot be presented here due to the insignificant  $NO$  soil emissions at the experimental site.

Moreover, we determined a median net chemical  $O_3$  production of 10 % during daytime within the air column between the EC flux measurement and the canopy, which was due to the absence of soil biogenic  $NO$  emission in our study. Hence, in contrast to previous studies our measured  $O_3$  deposition flux by EC is slightly underestimated. The chemical flux divergence for  $O_3$  was one order of magnitude larger during the high  $NO_x$  than during the low  $NO_x$  periods. In-canopy Damköhler numbers were shown to be relevant for  $NO_2$  only under nighttime conditions, which was due to the minor role of  $NO_2$  uptake by plants at this time. Damköhler numbers above the canopy indicated a potential flux divergence, but did not provide a hint for the observed chemical production of  $O_3$ . The only instance without indication of a chemical flux divergence within the entire data set was found during nighttime of the high  $NO_x$  periods in the lowermost canopy layer.

**Acknowledgements.** This project was funded by the Max Planck Society. We are grateful to J.-C. Mayer for the installation and the maintenance of meteorological sensors and for supporting the data evaluation. We are indebted to A. Moravek for his support with the eddy covariance measurements and the corresponding data evaluation and the fruitful discussions on many details of this study.

The service charges for this open access publication have been covered by the Max Planck Society.

Edited by: X. Wang

## References

- Atkinson, R. and Arey, J.: Gas-phase tropospheric chemistry of biogenic volatile organic compounds: a review, *Atmos. Environ.*, 37, S197–S219, 2003.
- Atkinson, R., Baulch, D. L., Cox, R. A., Crowley, J. N., Hampson, R. F., Hynes, R. G., Jenkin, M. E., Rossi, M. J., and Troe, J.:

- Evaluated kinetic and photochemical data for atmospheric chemistry: Volume I – gas phase reactions of  $O_x$ ,  $HO_x$ ,  $NO_x$  and  $SO_x$  species, *Atmos. Chem. Phys.*, 4, 1461–1738, doi:10.5194/acp-4-1461-2004, 2004.
- Aylor, D. E., Wang, Y. S., and Miller, D. R.: Intermittent wind close to the ground within a grass canopy, *Bound.-Lay. Meteorol.*, 66, 427–448, 1993.
- Bakwin, P. S., Wofsy, S. C., Fan, S. M., Keller, M., Trumbore, S. E., and Dacosta, J. M.: Emission of nitric-oxide (NO) from tropical forest soils and exchange of NO between the forest canopy and atmospheric boundary-layers, *J. Geophys. Res.-Atmos.*, 95, 16755–16764, 1990.
- Baldocchi, D.: A multi-layer model for estimating sulfur-dioxide deposition to a deciduous oak forest canopy, *Atmos. Environ.*, 22, 869–884, 1988.
- Breuninger, C., Oswald, R., Kesselmeier, J., and Meixner, F. X.: The dynamic chamber method: trace gas exchange fluxes ( $NO$ ,  $NO_2$ ,  $O_3$ ) between plants and the atmosphere in the laboratory and in the field, *Atmos. Meas. Tech.*, 5, 955–989, doi:10.5194/amt-5-955-2012, 2012.
- Crutzen, P.: Discussion of chemistry of some minor constituents in stratosphere and troposphere, *Pure Appl. Geophys.*, 106, 1385–1399, 1973.
- Denmead, O. T., Freney, J. R., and Dunin, F. X.: Gas exchange between plant canopies and the atmosphere: Case-studies for ammonia, *Atmos. Environ.*, 42, 3394–3406, 2007.
- Dorsey, J. R., Duyzer, J. H., Gallagher, M. W., Coe, H., Pilegaard, K., Weststrate, J. H., Jensen, N. O., and Walton, S.: Oxidized nitrogen and ozone interaction with forests, I: Experimental observations and analysis of exchange with Douglas fir, *Q. J. Roy Meteor. Soc.*, 130, 1941–1955, 2004.
- Dupont, S. and Patton, E. G.: Momentum and scalar transport within a vegetation canopy following atmospheric stability and seasonal canopy changes: the CHATS experiment, *Atmos. Chem. Phys.*, 12, 5913–5935, doi:10.5194/acp-12-5913-2012, 2012.
- Duyzer, J. H., Deinum, G., and Baak, J.: The interpretation of measurements of surface exchange of nitrogen-oxides – correction for chemical-reactions, *Philos. T. R. Soc. A*, 351, 231–248, 1995.
- Erisman, J. W., Vanpul, A., and Wyers, P.: Parametrization of the surface-resistance for the quantification of atmospheric deposition of acidifying pollutants and ozone, *Atmos. Environ.*, 28, 2595–2607, 1994.
- Finnigan, J.: Turbulence in plant canopies, *Annu. Rev. Fluid Mech.*, 32, 519–571, 2000.
- Foken, T.: *Micrometeorology*, Springer, Berlin, Heidelberg, 306 pp., 2008.
- Foken, T., Meixner, F. X., Falge, E., Zetzsch, C., Serafimovich, A., Bargsten, A., Behrendt, T., Biermann, T., Breuninger, C., Dix, S., Gerken, T., Hunner, M., Lehmann-Pape, L., Hens, K., Jocher, G., Kesselmeier, J., Luers, J., Mayer, J. C., Moravek, A., Plake, D., Riederer, M., Rutz, F., Scheibe, M., Siebicke, L., Sörgel, M., Staudt, K., Trebs, I., Tsokankunku, A., Welling, M., Wolff, V., and Zhu, Z.: Coupling processes and exchange of energy and reactive and non-reactive trace gases at a forest site – results of the EGER experiment, *Atmos. Chem. Phys.*, 12, 1923–1950, doi:10.5194/acp-12-1923-2012, 2012.
- Ganzeveld, L., Ammann, C., and Loubet, B.: Review on modelling atmosphere biosphere ex-change of Ozone and Nitrogen oxides. Background document for the joint ÉCLAIRE/COST ES0804 Expert Workshop “From process scale to global scale: integrating our knowledge on biosphere/atmosphere exchange modelling of trace gases and volatile aerosols”, 2012.
- Gut, A., Scheibe, M., Rottenberger, S., Rummel, U., Welling, M., Ammann, C., Kirkman, G. A., Kuhn, U., Meixner, F. X., Kesselmeier, J., Lehmann, B. E., Schmidt, W., Müller, E., and Piedade, M. T. F.: Exchange fluxes of  $NO_2$  and  $O_3$  at soil and leaf surfaces in an Amazonian rain forest, *J. Geophys. Res.-Atmos.*, 107, 8060, doi:10.1029/2001JD000654, 2002.
- Hänsel, H. and Neumann, W.: *Physik*, Spektrum, Akad. Verl., Heidelberg, Berlin, Oxford, 1995.
- Heal, M. R., Booth, B. B. B., Cape, J. N., and Hargreaves, K. J.: The influence of simplified peroxy radical chemistry on the interpretation of  $NO_2$ - $NO$ - $O_3$  surface exchange, *Atmos. Environ.*, 35, 1687–1696, 2001.
- Hicks, B. B., Baldocchi, D. D., Meyers, T. P., Hosker, R. P., and Matt, D. R.: A preliminary multiple resistance routine for deriving dry deposition velocities from measured quantities, *Water Air Soil Poll.*, 36, 311–330, 1987.
- Högström, U.: Non-dimensional wind and temperature profiles in the atmospheric surface-layer – a re-evaluation, *Bound.-Lay. Meteorol.*, 42, 55–78, 1988.
- Holzinger, R., Lee, A., Paw, K. T., and Goldstein, U. A. H.: Observations of oxidation products above a forest imply biogenic emissions of very reactive compounds, *Atmos. Chem. Phys.*, 5, 67–75, doi:10.5194/acp-5-67-2005, 2005.
- IPCC: Climate Change 2013: the physical science basis. Working group I contribution to the fifth assessment report of the Intergovernmental Panel on Climate Change, University Press, Cambridge, UK, 2013.
- Jacob, D. J. and Wofsy, S. C.: Budgets of reactive nitrogen, hydrocarbons, and ozone over the amazon-forest during the wet season, *J. Geophys. Res.-Atmos.*, 95, 16737–16754, 1990.
- Jacobs, A. F. G., Vanboxel, J. H., and Elkilani, R. M. M.: Nighttime free-convection characteristics within a plant canopy, *Bound.-Lay. Meteorol.*, 71, 375–391, 1994.
- Jäggi, M., Ammann, C., Neftel, A., and Fuhrer, J.: Environmental control of profiles of ozone concentration in a grassland canopy, *Atmos. Environ.*, 40, 5496–5507, 2006.
- Kasanko, M., Palmieri, A., and Coyette, C.: Land cover/ land use statistics, in: *Agriculture and Fishery Statistics*, edited by: Coyette, C., and Schenk, H., Eurostat, Luxembourg, 158, 2011.
- Kruijt, B., Malhi, Y., Lloyd, J., Norbre, A. D., Miranda, A. C., Pereira, M. G. P., Culf, A., and Grace, J.: Turbulence statistics above and within two Amazon rain forest canopies, *Bound.-Lay. Meteorol.*, 94, 297–331, 2000.
- Kurpius, M. R. and Goldstein, A. H.: Gas-phase chemistry dominates  $O_3$  loss to a forest, implying a source of aerosols and hydroxyl radicals to the atmosphere, *Geophys. Res. Lett.*, 30, 1371, doi:10.1029/2002gl016785, 2003.
- Lamaud, E., Loubet, B., Irvine, M., Stella, P., Personne, E., and Cellier, P.: Partitioning of ozone deposition over a developed maize crop between stomatal and non-stomatal uptakes, using eddy-covariance flux measurements and modelling, *Agr. Forest Meteorol.*, 149, 1385–1396, 2009.
- Lehmann, B. E., Lehmann, M., Neftel, A., Gut, A., and Tarakanov, S. V.: Radon-220 calibration of near-surface turbulent gas transport, *Geophys. Res. Lett.*, 26, 607–610, 1999.

- Lenschow, D. H.: Reactive trace species in the boundary-layer from a micrometeorological perspective, *J. Meteorol. Soc. Jpn.*, 60, 472–480, 1982.
- Lerdau, M. T., Munger, L. J., and Jacob, D. J.: Atmospheric chemistry - the NO<sub>2</sub> flux conundrum, *Science*, 289, 2291, doi:10.1126/science.289.5488.2291, 2000.
- Mauder, M. and Foken, T.: Documentation and instruction manual of the eddy-covariance software package TK3, *Arbeitsergebnisse* Nr. 46, 2011.
- Monsi, M. and Saeki, T.: Über den Lichtfaktor in den Pflanzengesellschaften und seine Bedeutung für die Stoffproduktion, *Jpn. J. Botany*, 14, 22–52, 1953.
- Monteith, J. L. and Unsworth, M. H.: Principles of environmental physics, 2nd ed., E. Arnold, London, New York, 291 pp., 1990.
- Moravek, A., Foken, T., and Trebs, I.: Application of a GC-ECD for measurements of biosphere-atmosphere exchange fluxes of peroxyacetyl nitrate using the relaxed eddy accumulation and gradient method, *Atmos. Meas. Tech.*, 7, 2097–2119, doi:10.5194/amt-7-2097-2014, 2014.
- Moravek, A., Stella, P., Foken, T., and Trebs, I.: Influence of local air pollution on the deposition of peroxyacetyl nitrate to a nutrient-poor natural grassland ecosystem, *Atmos. Chem. Phys.*, 15, 899–911, doi:10.5194/acp-15-899-2015, 2015.
- Nemitz, E., Sutton, M. A., Gut, A., San Jose, R., Husted, S., and Schjoerring, J. K.: Sources and sinks of ammonia within an oilseed rape canopy, *Agr. Forest Meteorol.*, 105, 385–404, 2000.
- Nemitz, E., Loubet, B., Lehmann, B. E., Cellier, P., Neftel, A., Jones, S. K., Hensen, A., Ihly, B., Tarakanov, S. V., and Sutton, M. A.: Turbulence characteristics in grassland canopies and implications for tracer transport, *Biogeosciences*, 6, 1519–1537, doi:10.5194/bg-6-1519-2009, 2009.
- Personne, E., Loubet, B., Herrmann, B., Mattsson, M., Schjoerring, J. K., Nemitz, E., Sutton, M. A., and Cellier, P.: SURFATM-NH<sub>3</sub>: a model combining the surface energy balance and bi-directional exchanges of ammonia applied at the field scale, *Biogeosciences*, 6, 1371–1388, doi:10.5194/bg-6-1371-2009, 2009.
- Plake, D. and Trebs, I.: An automated system for selective and continuous measurements of vertical thoron profiles for the determination of transport times near the ground, *Atmos. Meas. Tech.*, 6, 1017–1030, doi:10.5194/amt-6-1017-2013, 2013.
- Plake, D., Stella, P., Moravek, A., Mayer, J. C., Ammann, C., Held, A., and Trebs, I.: Comparison of ozone deposition measured with the dynamic chamber and the eddy covariance method, *Agr. Forest Meteorol.*, submitted, 2014.
- Rinne, J., Markkanen, T., Ruuskanen, T. M., Petaja, T., Keronen, P., Tang, M. J., Crowley, J. N., Rannik, U., and Vesala, T.: Effect of chemical degradation on fluxes of reactive compounds – a study with a stochastic Lagrangian transport model, *Atmos. Chem. Phys.*, 12, 4843–4854, doi:10.5194/acp-12-4843-2012, 2012.
- Ripley, E. A. and Redman, R. E.: Grassland, in: *Vegetation and the atmosphere*, edited by: Monteith, J. L., Acad. Press, London, 1976.
- Rummel, U.: Turbulent exchange of ozone and nitrogen oxides between an Amazonian rain forest and the atmosphere, PhD thesis, Faculty of Biology, Chemistry and Geosciences, University of Bayreuth, Bayreuth, 246 pp., 2005.
- Rummel, U., Ammann, C., Gut, A., Meixner, F. X., and Andreae, M. O.: Eddy covariance measurements of nitric oxide flux within an Amazonian rain forest, *J. Geophys. Res.-Atmos.*, 107, 8050, doi:10.1029/2001jd000520, 2002.
- Rummel, U., Ammann, C., Kirkman, G. A., Moura, M. A. L., Foken, T., Andreae, M. O., and Meixner, F. X.: Seasonal variation of ozone deposition to a tropical rain forest in southwest Amazonia, *Atmos. Chem. Phys.*, 7, 5415–5435, 2007, <http://www.atmos-chem-phys.net/7/5415/2007/>.
- Seinfeld, J. H. and Pandis, S. N.: *Atmospheric chemistry and physics : from air pollution to climate change*, 2. Edn., Wiley, Hoboken, NJ, 1203 pp., 2006.
- Simon, E., Lehmann, B. E., Ammann, C., Ganzeveld, L., Rummel, U., Meixner, F. X., Nobre, A. D., Araujo, A., and Kesselmeier, J.: Lagrangian dispersion of Rn-222, H<sub>2</sub>O and CO<sub>2</sub> within Amazonian rain forest, *Agr. Forest Meteorol.*, 132, 286–304, 2005.
- Stella, P., Kortner, M., Ammann, C., Foken, T., Meixner, F. X., and Trebs, I.: Measurements of nitrogen oxides and ozone fluxes by eddy covariance at a meadow: evidence for an internal leaf resistance to NO<sub>2</sub>, *Biogeosciences*, 10, 5997–6017, doi:10.5194/bg-10-5997-2013, 2013.
- Suttie, J. M., Reynolds, S. G., and Batello, C.: Introduction, in: *Grasslands of the world*, edited by: Suttie, J. M., Reynolds, S. G., and Batello, C., FAO, Rome, 2005.
- Swinbank, W. C.: A comparison between predictions of dimensional analysis for constant-flux layer and observations in unstable conditions, *Q. J. Roy Meteor. Soc.*, 94, 460–467, 1968.
- Trebs, I., Bohn, B., Ammann, C., Rummel, U., Blumthaler, M., Königstedt, R., Meixner, F. X., Fan, S., and Andreae, M. O.: Relationship between the NO<sub>2</sub> photolysis frequency and the solar global irradiance, *Atmos. Meas. Tech.*, 2, 725–739, doi:10.5194/amt-2-725-2009, 2009.
- Trebs, I., Mayol-Bracero, O. L., Pauliquevis, T., Kuhn, U., Sander, R., Ganzeveld, L., Meixner, F. X., Kesselmeier, J., Artaxo, P. and Andreae, M. O.: Impact of the Manaus urban plume on trace gas mixing ratios near the surface in the Amazon Basin: Implications for the NO-NO<sub>2</sub>-O<sub>3</sub> photostationary state and peroxy radical levels, *J. Geophys. Res.*, 117, D05307, doi:10.1029/2011JD016386, 2012.
- Trumbore, S. E., Keller, M., Wofsy, S. C., and Dacosta, J. M.: Measurements of soil and canopy exchange-rates in the Amazon rain-forest using Rn-222, *J. Geophys. Res.-Atmos.*, 95, 16865–16873, 1990.
- van Pul, W. A. J., and Jacobs, A. F. G.: The conductance of a maize crop and the underlying soil to ozone under various environmental-conditions, *Bound.-Lay. Meteorol.*, 69, 83–99, 1994.
- Warneck, P.: *Chemistry of the natural atmosphere*, 2nd ed., Academic Press, San Diego, California, 927 pp., 2000.
- Wolfe, G. M., Cantrell, C., Kim, S., Mauldin III, R. L., Karl, T., Harley, P., Turnipseed, A., Zheng, W., Flocke, F., Apel, E. C., Hornbrook, R. S., Hall, S. R., Ullmann, K., Henry, S. B., DiGangi, J. P., Boyle, E. S., Kaser, L., Schnitzhofer, R., Hansel, A., Gaus, M., Nakashima, Y., Kajii, Y., Guenther, A., and Keutsch, F. N.: Missing per-oxy radical sources within a summertime ponderosa pine forest, *Atmos. Chem. Phys.*, 14, 4715–4732, doi:10.5194/acp-14-4715-2014, 2014.
- Yienger, J. J. and Levy, H.: Empirical-model of global soil-biogenic NO<sub>x</sub> emissions, *J. Geophys. Res.-Atmos.*, 100, 11447–11464, 1995.